Nonreciprocity Realized with Quantum Nonlinearity

Andrés Rosario Hamann,[1,*] Clemens Müller,[1,2] Markus Jerger,[1] Maximilian Zanner,[3] Joshua Combes,[1] Mikhail Pletyukhov,[4] Martin Weides,[3,5] Thomas M. Stace,[1] and Arkady Fedorov[1,†]

[1]*ARC Centre of Excellence for Engineered Quantum Systems, School of Mathematics and Physics, The University of Queensland, Saint Lucia, Queensland 4072, Australia*

[2]*Institute for Theoretical Physics, ETH Zürich, 8093 Zürich, Switzerland*

[3]*Physikalisches Institut, Karlsruhe Institute of Technology (KIT), 76131 Karlsruhe, Germany*

[4]*Institute for Theory of Statistical Physics, RWTH Aachen University, 52056 Aachen, Germany*

[5]*School of Engineering, Electronics & Nanoscale Engineering Division, University of Glasgow, Glasgow G12 8QQ, United Kingdom*

(Received 8 July 2018; published 17 September 2018)

Nonreciprocal devices are a key element for signal routing and noise isolation. Rapid development of quantum technologies has boosted the demand for a new generation of miniaturized and low-loss nonreciprocal components. Here, we use a pair of tunable superconducting artificial atoms in a 1D waveguide to experimentally realize a minimal passive nonreciprocal device. Taking advantage of the quantum nonlinear behavior of artificial atoms, we achieve nonreciprocal transmission through the waveguide in a wide range of powers. Our results are consistent with theoretical modeling showing that nonreciprocity is associated with the population of the two-qubit nonlocal entangled quasidark state, which responds asymmetrically to incident fields from opposing directions. Our experiment highlights the role of quantum correlations in enabling nonreciprocal behavior and opens a path to building passive quantum nonreciprocal devices without magnetic fields.

DOI: 10.1103/PhysRevLett.121.123601

Microwave nonreciprocal devices based on ferromagnetic compounds increase signal processing capabilities, but they are bulky and inherently lossy [1]. Different approaches to achieve nonreciprocity on a chip are being actively pursued to enable circuits of greater complexity and advanced functionality. A common path to achieve nonreciprocity consists in breaking time-reversal symmetry, either by utilizing novel materials [2–4] or by exploiting sophisticated time control schemes [5–10]. Here, we follow another path and use a pair of tunable superconducting artificial atoms in a 1D waveguide in order to realize the simplest possible nonreciprocal device without breaking time-reversal symmetry. In contrast to isolators based on nonlinear bulk media response [11,12], nonlinear resonances [13], or nonlinearity enhanced by active breaking of the parity-time symmetry [14], our system exploits the quantum nonlinear behavior of a minimal system comprised of two two-level artificial atoms [15–18]. This quantum nonlinearity, combined with an asymmetric atomic detuning that breaks the structural symmetry of the system, leads to population trapping of an entangled state and, ultimately, to 15 dB isolation in a wide range of powers controllable by the experimental settings. Our experiment provides insights into the role of quantum correlations in generating nonreciprocity and opens a new path towards the realization of nonreciprocal quantum devices on a chip.

Schemes for building nonreciprocal devices based on nonlinearity of quantum emitters were first proposed in Refs. [19,20]. A more specific implementation of a *quantum diode* built of two atoms in 1D open space was later proposed in Ref. [15] and has attracted significant theoretical attention since [9,16–18,21]. The quantum theory of the diode was first presented in Refs. [9,16,17] and later work revealed the detailed mechanism of nonreciprocity, determining analytical bounds for the device efficiency and identifying entanglement between the atoms and the electromagnetic field as a crucial element in the nonreciprocal behavior of the system [18]. In this work, we present experimental results on the realization of the quantum diode and provide compelling evidence of the connection of its nonreciprocity with the population of the entangled quasidark state.

More specifically, we use two transmon-type superconducting qubits inserted in a rectangular copper waveguide [see Fig. 1(c)]. The qubits are spatially separated by $d = 22.5$ mm and are oriented to maximize coupling to the TE_{10} mode, which has a lower cutoff at $f_{c,10} = 6.55$ GHz. Two microwave connectors are positioned near each end of the waveguide, providing an interface between the microwave field inside the waveguide and the external circuitry. This ensures that the qubits are coupled to the continuum of the electromagnetic modes, thus emulating an effective 1D open space. The qubits consist of two planar capacitor

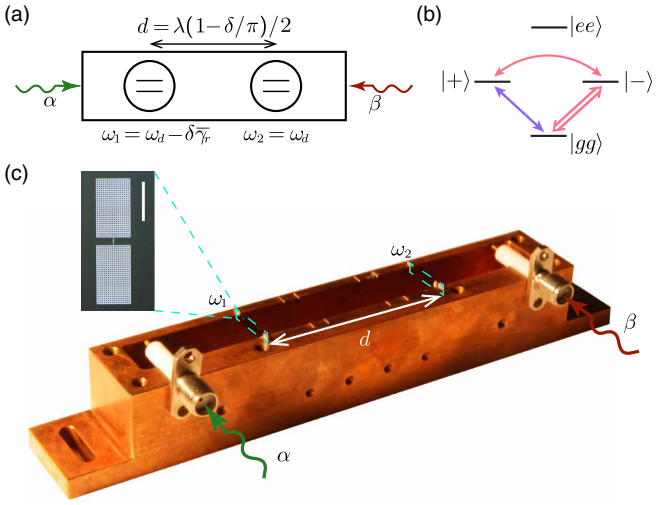

FIG. 1. (a) Schematic of the quantum diode: two qubits embedded in a 1D waveguide, tuned to the optimal conditions for nonreciprocal behavior ($\omega_1 = \omega_d - \delta\bar{\gamma}_r$, $\omega_2 = \omega_d$). An incoming field from the forward direction (α drive) at frequency ω_d is partially transmitted through the system, whereas a field incoming from the reverse direction (β drive) is fully reflected. (b) Energy level diagram of the system. The quasidark state $|+\rangle$ can be populated by the driving field either directly from the ground state $|gg\rangle$ (purple path) or indirectly through the bright state $|-\rangle$ (pink path). These two channels interfere either constructively or destructively depending on the driving direction. If interfering constructively, part of the population gets trapped in the quasidark state $|+\rangle$, which in turn gives rise to the nonreciprocal behavior of the system. (c) Open 1D waveguide with embedded 3D transmons (dashed mint green boxes). Inset: Optical micrograph of one of the two identical 3D transmons. The scale bar corresponds to 500 μm.

plates connected via a line interrupted by a SQUID, playing the role of a tunable Josephson junction [see inset Fig. 1(c)]. The transition frequencies of the qubits are then controlled via two superconducting coils. Further technical details into the transmons and waveguide design and characterization can be found in the Supplemental Material [22] and Ref. [24].

As a result of the interaction with the waveguide modes, the excited state of a qubit $|e\rangle$ spontaneously relaxes to its ground state $|g\rangle$ at the radiative decay rate $\gamma_r/2\pi$. This interaction leads to an almost full reflection of incident resonant microwaves by the qubit at low powers [25], a phenomenon we use to determine the frequency of our qubits, their radiative decay rates, and their decoherence due to other noise channels (refer to the Supplemental Material for more details [22]). The rates $\gamma_r/2\pi$ were found to depend on the transition frequencies of the qubits f_{ge}, and varied between 60 and 85 MHz for f_{ge} between 8.5 and 9.0 GHz, respectively. The transmittance at resonance with the qubit was extinguished to less than 0.4% at low powers of incident radiation, providing an upper bound on the qubits' decoherence rate. This is characterized by the nonradiative decay $\gamma_{\rm nr}$ and dephasing γ_ϕ rates, which we measured to fall below $0.5\%\gamma_r$ for both qubits.

When the two-atom system is driven by an external microwave field, their interaction depends strongly on the distance between qubits. Specifically, the interatomic distance d determines the phase ϕ acquired by the drive when traveling from one qubit to the other, $\phi = \omega_d d/v_p$, where v_p is the phase velocity in the waveguide and ω_d is the frequency of the drive. We tune ϕ *in situ* by setting the frequency ω_d of the incoming drive.

This interaction between the two qubits with the continuum of the electromagnetic modes in the waveguide gives rise to a field mediated exchange coupling between the qubits described via the term [26] $H_C = \frac{1}{2}\bar{\gamma}_r \sin\phi(\sigma_-^{(1)}\sigma_+^{(2)} + \text{H.c.})$, where $\sigma_- = |g\rangle\langle e|$ and $\bar{\gamma}_r \equiv \sqrt{\gamma_{r,1}\gamma_{r,2}}$ (see Supplemental Material [22]). At the phase matching condition $\phi = \pi$ (which, in the case of our system occurs when $\omega_d = \omega_\pi$, with $\omega_\pi \equiv 8.975$ GHz), the exchange coupling between the qubits vanishes, as the qubit interactions with the continuum of photonic modes above and below the qubit frequency cancel each other [26,27]. In this case, the symmetric and antisymmetric states $|\pm\rangle = (|ge\rangle \pm |eg\rangle)/\sqrt{2}$ are perfectly degenerate. Furthermore, the antisymmetric state $|-\rangle$ is bright, with a decay rate $\Gamma_- = 2\bar{\gamma}_r$, whereas the symmetric state $|+\rangle$ is dark, and hence fully decoupled from the interaction with the waveguide modes: $\Gamma_+ = 0$ [26].

If the qubits are slightly detuned from the frequency ω_π, a resonant field at ω_d acquires a phase $\phi = (\omega_d/\omega_\pi)\pi \equiv \pi - \delta$, where the small parameter $\delta \ll 1$ characterizes the detuning from the phase matching condition. In this case, the exchange interaction between qubits does not vanish and lifts in turn the degeneracy between the $|\pm\rangle$ states: $H_C = (J/2)(\sigma_+^{(1)}\sigma_-^{(2)} + \text{H.c.})$, with $J = \bar{\gamma}_r \sin\phi \simeq \bar{\gamma}_r\delta$. To leading order in δ, the dark state $|+\rangle$ becomes quasidark with a decay rate $\Gamma_+ = \delta^2\bar{\gamma}_r$, while the bright state decay rate remains unchanged: $\Gamma_- = 2\bar{\gamma}_r$, [18,28].

To break the inversion symmetry of our device and achieve nonreciprocal behavior, we set qubit 2 to be resonant with the incoming field, $\omega_2 = \omega_d$, whereas qubit 1 is set at $\omega_1 = \omega_d - \delta\bar{\gamma}_r$, to compensate for the phase asymmetry introduced by the detuned ω_d [see Fig. 1(a)]. This configuration opens an additional path of accessing the quasidark state $|+\rangle$, which can now be populated either directly by the incoming field ($|gg\rangle \leftrightarrow |+\rangle$) or indirectly through the bright state ($|gg\rangle \leftrightarrow |-\rangle \leftrightarrow |+\rangle$), to which it is coupled via the exchange term [Fig. 1(b)].

Our measurement setup allows us to drive the system from either the forward or reverse direction [α and β driving, respectively, in Fig. 1(a)], with the reflected and transmitted fields simultaneously detected at both sides (refer to the Supplemental Material [22] for extra details on the measurement setup). When driving in the forward direction, both channels to populate the quasidark state

$|+\rangle$ interfere constructively, giving rise to an excitation of $|+\rangle$. Neglecting nonradiative decay and dephasing ($\gamma_{\rm nr} = \gamma_\phi = 0$), the resulting steady state solution for the density operator of the qubits can be found analytically [18] as $\rho_{\rm st} = (1/3)|gg\rangle\langle gg| + (2/3)|+\rangle\langle +| + O(\delta^2)$ for intermediate driving powers $\delta^2\bar{\gamma}_r \ll p \ll 2\bar{\gamma}_r$. Under these conditions, the system is predominantly trapped in the quasidark state $|+\rangle$ and is therefore partially transparent to the incident signal, due to the extremely low saturability of $|+\rangle$.

If the system is driven in the reverse direction, both channels interfere destructively, the quasidark state remains unpopulated, and the steady state solution is given by $\rho_{\rm st} = |gg\rangle\langle gg| + O(\delta^2)$ for powers $p \ll 2\bar{\gamma}_r$. In this case, the incoming signal is reflected by the bright state and the two-qubit system behaves as a mirror.

To illustrate the mechanism of nonreciprocal transmission, we tune the system to its optimal nonreciprocal configuration (up to experimental uncertainties) for two different values of the parameter δ: $\delta^2 \simeq 10^{-2}$ and $\delta^2 \simeq 10^{-3}$, corresponding to driving frequencies $\omega_d \simeq 8.8358$ GHz and $\omega_d \simeq 8.6188$ GHz, respectively. For each case, we measure the transmission amplitude in both the forward and reverse driving direction.

By controlling the driving power, we are able to probe three characteristic regimes of the device, featured in Fig. 2:

(i) In the low power regime, $p/\bar{\gamma}_r \ll \delta^2$, the device behaves reciprocally, reflecting most of the incoming radiation. In this regime, the degree of transmission suppression is only limited by the qubits' decoherence and relaxation rates, and by the accuracy of qubit tuning to ensure that $\omega_2 = \omega_d$.

(ii) In the intermediate power regime, $\delta^2 \ll p/\bar{\gamma}_r \ll 1$, the transmission amplitude in the forward direction $t_\rightarrow$ increases and features the characteristic plateau predicted by theory [16,18]. The transmission amplitude in the reverse direction $t_\leftarrow$ remains near zero independently of the value of $p/\bar{\gamma}_r$ and the system behaves nonreciprocally.

(iii) In the high power regime, $p/\bar{\gamma}_r \gg 1$, the bright state saturates, regardless of the driving direction, and the system returns to its reciprocal behavior.

The power range over which the device behaves nonreciprocally (plateau in Fig. 2) can be extended by decreasing δ. However, decreasing δ also reduces the lifetime of the quasidark state $|+\rangle$, which leads to a corresponding decrease in the bandwidth of the diode.

In order to provide a metric of the isolation capabilities of the quantum diode, we calculate the *diode efficiency* $\mathcal{E} \equiv |t_\rightarrow|(|t_\rightarrow| - |t_\leftarrow|)/(|t_\rightarrow| + |t_\leftarrow|)$ used in Ref. [16] which, in the ideal case of identical qubits and no decoherence, coincides with the definition of efficiency used in Refs. [15–17]. In spite of relatively low dephasing and nonradiative decay rates (γ_ϕ, $\gamma_{\rm nr} < 0.5\%\gamma_r$ for both qubits), the maximum diode efficiency appears to be limited to $\simeq$0.27, well below its ideal value [18] of 2/3

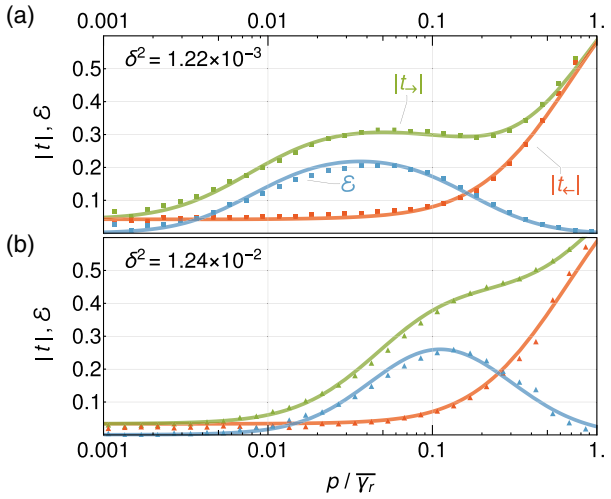

FIG. 2. Nonreciprocity dependence on power. Experimental data (points) and theoretical fits (solid lines) for the forward driving transmission amplitude $|t_\rightarrow|$ (green), reverse driving transmission amplitude $|t_\leftarrow|$ (red), and diode efficiency $\mathcal{E}$ (blue). $\mathcal{E} \equiv |t_\rightarrow|(|t_\rightarrow| - |t_\leftarrow|)/(|t_\rightarrow| + |t_\leftarrow|)$ measures the nonreciprocal behavior of the system as well as its forward transmitting capabilities. The system is tuned to its optimal nonreciprocal configuration for two different detunings: (a) $\delta^2 \simeq 0.001$, (b) $\delta^2 \simeq 0.01$. In both cases the device behaves reciprocally and reflects most of the incoming radiation at the low power regime $p/\bar{\gamma}_r \ll \delta^2$. However, as the power increases past the onset of the diode regime, indicated by δ^2, saturation of the quasidark state allows for an increase in $|t_\rightarrow|$, while $|t_\leftarrow|$ remains unchanged.

(see Fig. 2). This illustrates an experimental challenge in the realization of the quantum diode: since the nonreciprocal behavior relies on populating the quasidark state $|+\rangle$, the transition rate relevant for the system dynamics is $\Gamma_+ = \delta^2\bar{\gamma}_r \ll \bar{\gamma}_r$. In our experiment, the dephasing and dissipation rates, γ_ϕ, $\gamma_{\rm nr}$, are of the same order of magnitude of Γ_+. This renders the effect of decoherence much more significative compared to single-qubit phenomena, whose dynamics evolve at the much faster rate γ_r.

Further insights into the role of the quasidark state can be obtained by measuring the full spectrum of the elastically and inelastically scattered radiation. We set the atomic detunings and driving power to the values that maximize the diode efficiency and then measure power spectral densities when driving the system in both the forward and reverse directions. Notably, the measurement of the power spectral densities, in addition to a δ-like peak due to elastically (Rayleigh) scattered radiation (Fig. 3), features an additional broader peak, which we identify with radiation inelastically scattered off the quasidark $|+\rangle$ state. The measured power spectrum agrees with our expectation of the total scattered power being a measure of the population of the quasidark state: as clearly seen from the measurement (Fig. 3), the scattered power is much greater when the system is driven in the forward direction.

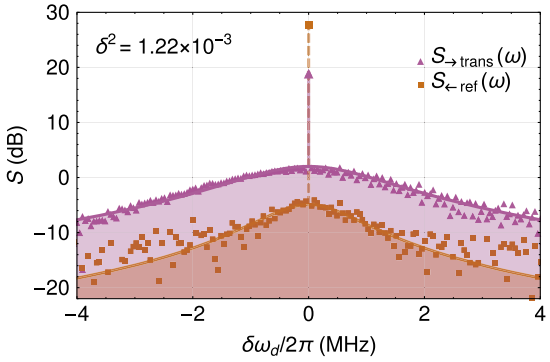

FIG. 3. Power spectral densities of the forward driving transmitted field $[S_{\rightarrow\mathrm{trans}}(\omega)]$ and the reverse driving reflected field $[S_{\leftarrow\mathrm{ref}}(\omega)]$. Both spectra were taken after tuning the device to its optimum nonreciprocal configuration for $\delta^2 \simeq 0.001$ [as in Fig. 2(a)] and setting the driving power such that the diode efficiency $\mathcal{E}$ is maximum [corresponding to $p/\bar{\gamma}_r \simeq 0.05$ in Fig. 2(a)]. Both scattered fields travel through the same amplification chain. The δ-like peaks at the driving frequency ω_d correspond to the elastically scattered fields. Radiation inelastically scattered off the quasidark state $|+\rangle$ generates an additional broader peak, which we fit to Lorentzians of width $\gamma_{\rightarrow\mathrm{trans}} = 2.92$ MHz and $\gamma_{\leftarrow\mathrm{ref}} = 1.76$ MHz (solid lines). When driving the system in the forward direction, part of the population gets trapped in the quasidark state, consistent with a greater inelastically scattered radiation power: $\int S_{\rightarrow\mathrm{trans}} d\omega \gg \int S_{\leftarrow\mathrm{ref}} d\omega$.

Being able to control δ, we can tune the linewidth of the dark state emission, $\Gamma_+ = \delta^2\bar{\gamma}_r$. Figure 4 shows the power spectral densities of scattered radiation for three values of δ (here the elastic part has been omitted for clarity).

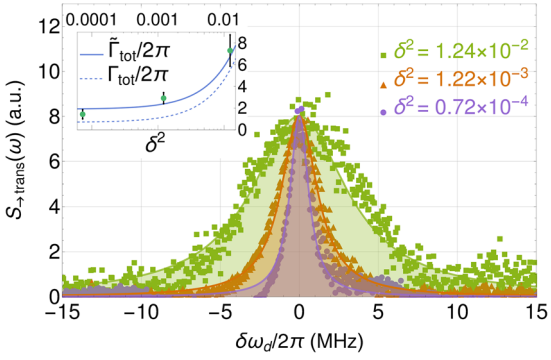

FIG. 4. Power spectral densities of the inelastically scattered transmitted field. The system is driven in the forward direction for different detuning regimes ($\delta^2 \simeq 0.01$, 0.001, 0.0001). In every case, the spectra were taken at the optimum atomic detunings and driving powers that maximize the diode efficiency $\mathcal{E}$. The solid lines are fits to Lorentzians of width 1.43, 2.92, and 7.30 MHz, in increasing order of δ^2. As predicted by theory, the linewidth $\Gamma_{\mathrm{FWHM}} \equiv 2(3\delta^2\bar{\gamma}_r + 2\gamma_\phi + \gamma_{\mathrm{nr}})$ of the scattered field increases linearly with δ^2 (see inset). However, in the experiment the width of the inelastically scattered radiation is broader than expected: $\tilde{\Gamma}_{\mathrm{tot}} = \Gamma_{\mathrm{tot}} + \Gamma_{\mathrm{exc}}$, with $\Gamma_{\mathrm{exc}}/2\pi = 1.22$ MHz. The elastic part of the scattered radiation at $\delta\omega_d = 0$ MHz has been omitted and the peaks are scaled for clarity.

As expected, the linewidth of the fluorescence spectra increases linearly with δ^2, following the increase in the decay rate of the dark state.

Our theoretical estimates predict that the width of the emission peak results from a combination of the dark state linewidth Γ_+ and broadening due to nonradiative and dephasing contributions. In the optimal diode conditions, the linewidth of the transmitted field when driving the system in the forward direction can be found analytically as $\Gamma_{\mathrm{FWHM}} = 2(3\Gamma_+ + 2\gamma_\phi + \gamma_{\mathrm{nr}})$ (see Supplemental Material [22]). In the experiment, the width of the inelastically scattered radiation is wider than predicted by 1.22 MHz. This indicates an additional source of noise (presumably of technical origin) which could be mixed with the detected signal and results in an additional broadening of the scattered field.

The quantum diode is partially transparent to forward driving radiation because a substantial fraction of the system's population is trapped in the quasidark state $|+\rangle$. This finite population of $|+\rangle$ unavoidably leads to inelastic scattering of the incoming radiation, which then contributes to insertion losses. However, inelastic scattering can be controlled via the detuning parameter δ, as shown in Fig. 4.

By incorporating quantum-limited Josephson parametric amplifiers into our detection lines [29], we can measure time-domain single-shot data of the scattered fields and calculate its statistics. Our results show that the in-phase noise is higher when driving the system in the forward direction than in the reverse direction (see Supplemental Material [22]). This is consistent with the statistics produced by replacing the system with a simple stochastic mirror, as theoretically predicted in Ref. [18].

In conclusion, we experimentally realized a passive quantum nonreciprocal device comprised of a minimal number of constituents. At least two localized quantum emitters are required to break structural symmetry in 1D space, while a two-level atom is the simplest system presenting a nonlinear quantum behavior. The nonreciprocity relies on the interplay of the exchange interaction and the collective decay of quantum emitters leading to population trapping into an entangled quasidark state for a preferred driving direction. It is instructive to note that our device breaks some of the fundamental bounds derived for classical nonlinear devices [13,30] but is not immune to the dynamic reciprocity limitations [31]. While not yet sufficient for practical applications, our results open a path for the realization of more efficient nonreciprocal devices with multiple coherent qubits. More specifically, we conjecture that the diode efficiency would scale as $n/(n+1)$, where n is the number of qubits embedded in the waveguide [18]. The demonstrated mechanism of population trapping is also valuable for the development of protocols of remote entanglement stabilization.

We thank Alexandre Roulet for useful discussions of our results and Shanhui Fan for helpful advise on dynamical reciprocity. We also thank Andrea Alù for reading

our manuscript and providing valuable insights into nonlinear nonreciprocity. This work was supported by the Australian Research Council under the Discovery and Centre of Excellence funding schemes (Projects No. DP150101033, No. DE160100356, and No. CE110001013), and UQ Foundation Research Excellence Award. M. W. acknowledges support from the European Research Council (ERC) under Grant Agreement No. 648011.

*arosario@uq.edu.au
†a.fedorov@uq.edu.au

[1] D. M. Pozar, *Microwave Engineering* (Wiley, Crawfordsville, 1998).
[2] G. Viola and D. P. DiVincenzo, Hall Effect Gyrators and Circulators, Phys. Rev. X **4**, 021019 (2014).
[3] A. C. Mahoney, J. I. Colless, S. J. Pauka, J. M. Hornibrook, J. D. Watson, G. C. Gardner, M. J. Manfra, A. C. Doherty, and D. J. Reilly, On-Chip Microwave Quantum Hall Circulator, Phys. Rev. X **7**, 011007 (2017).
[4] C. Müller, S. Guan, N. Vogt, J. H. Cole, and T. M. Stace, Passive On-Chip Superconducting Circulator Using a Ring of Tunnel Junctions, Phys. Rev. Lett. **120**, 213602 (2018).
[5] N. A. Estep, D. L. Sounas, J. Soric, and A. Alù, Magnetic-free non-reciprocity and isolation based on parametrically modulated coupled-resonator loops, Nat. Phys. **10**, 923 (2014).
[6] J. Kerckhoff, K. Lalumière, B. J. Chapman, A. Blais, and K. W. Lehnert, On-Chip Superconducting Microwave Circulator from Synthetic Rotation, Phys. Rev. Applied **4**, 034002 (2015).
[7] S. Barzanjeh, M. Wulf, M. Peruzzo, M. Kalaee, P. B. Dieterle, O. Painter, and J. M. Fink, Mechanical on-chip microwave circulator, Nat. Commun. **8**, 953 (2017).
[8] N. R. Bernier, L. D. Tóth, A. Koottandavida, M. A. Ioannou, D. Malz, A. Nunnenkamp, A. K. Feofanov, and T. J. Kippenberg, Nonreciprocal reconfigurable microwave optomechanical circuit, Nat. Commun. **8**, 604 (2017).
[9] K. Fang, J. Luo, A. Metelmann, M. H. Matheny, F. Marquardt, A. A. Clerk, and O. Painter, Generalized non-reciprocity in an optomechanical circuit via synthetic magnetism and reservoir engineering, Nat. Phys. **13**, 465 (2017).
[10] B. J. Chapman, E. I. Rosenthal, J. Kerckhoff, B. A. Moores, L. R. Vale, J. A. B. Mates, G. C. Hilton, K. Lalumière, A. Blais, and K. W. Lehnert, Widely Tunable On-Chip Microwave Circulator for Superconducting Quantum Circuits, Phys. Rev. X **7**, 041043 (2017).
[11] L. Fan, J. Wang, L. T. Varghese, H. Shen, B. Niu, Y. Xuan, A. M. Weiner, and M. Qi, An all-silicon passive optical diode, Science **335**, 447 (2012).
[12] Y. Yi, C. Yaohui, H. Hao, X. Weiqi, Y. Kresten, and M. Jesper, Nonreciprocal transmission in a nonlinear photonic-crystal Fano structure with broken symmetry, Laser Photonics Rev. **9**, 241 (2015).
[13] D. L. Sounas, J. Soric, and A. Alù, Broadband passive isolators based on coupled nonlinear resonances, Nat. Electronics **1**, 113 (2018).
[14] B. Peng, Ş. K. Özdemir, F. Lei, F. Monifi, M. Gianfreda, G. L. Long, S. Fan, F. Nori, C. M. Bender, and L. Yang, Parity-time-symmetric whispering-gallery microcavities, Nat. Phys. **10**, 394 (2014).
[15] F. Fratini, E. Mascarenhas, L. Safari, J. P. Poizat, D. Valente, A. Auffèves, D. Gerace, and M. F. Santos, Fabry-Perot Interferometer with Quantum Mirrors: Nonlinear Light Transport and Rectification, Phys. Rev. Lett. **113**, 243601 (2014).
[16] J. Dai, A. Roulet, H. N. Le, and V. Scarani, Rectification of light in the quantum regime, Phys. Rev. A **92**, 063848 (2015).
[17] F. Fratini and R. Ghobadi, Full quantum treatment of a light diode, Phys. Rev. A **93**, 023818 (2016).
[18] C. Müller, J. Combes, A. Rosario Hamann, A. Fedorov, and T. M. Stace, Nonreciprocal atomic scattering: A saturable, quantum Yagi-Uda antenna, Phys. Rev. A **96**, 053817 (2017).
[19] D. Roy, Few-photon optical diode, Phys. Rev. B **81**, 155117 (2010).
[20] D. Roy, Cascaded two-photon nonlinearity in a one-dimensional waveguide with multiple two-level emitters, Sci. Rep. **3**, 2337 (2013).
[21] E. Mascarenhas, M. F. Santos, A. Auffèves, and D. Gerace, Quantum rectifier in a one-dimensional photonic channel, Phys. Rev. A **93**, 043821 (2016).
[22] See Supplemental Material, http://link.aps.org/supplemental/10.1103/PhysRevLett.121.123601, for additional details into the measurement setup, fits, and additional calculations and measurements, which includes [23].
[23] J. Combes, J. Kerckhoff, and M. Sarovar, The SLH framework for modeling quantum input-output networks, Adv. Phys. X **2**, 784 (2017).
[24] M. Zanner, A. Rosario Hamann, L. Gruenhaupt, S. Diewald, A. Fedorov, A. V. Ustinov, and M. Weides (to be published).
[25] O. Astafiev, A. M. Zagoskin, A. A. Abdumalikov, Yu. A. Pashkin, T. Yamamoto, K. Inomata, Y. Nakamura, and J. S. Tsai, Resonance fluorescence of a single artificial atom, Science **327**, 840 (2010).
[26] K. Lalumière, B. C. Sanders, A. F. van Loo, A. Fedorov, A. Wallraff, and A. Blais, Input-output theory for waveguide QED with an ensemble of inhomogeneous atoms, Phys. Rev. A **88**, 043806 (2013).
[27] A. F. van Loo, A. Fedorov, K. Lalumière, B. C. Sanders, A. Blais, and A. Wallraff, Photon-mediated interactions between distant artificial atoms, Science **342**, 1494 (2013).
[28] E. S. Redchenko and V. I. Yudson, Decay of metastable excited states of two qubits in a waveguide, Phys. Rev. A **90**, 063829 (2014).
[29] C. Eichler, Y. Salathe, J. Mlynek, S. Schmidt, and A. Wallraff, Quantum-Limited Amplification and Entanglement in Coupled Nonlinear Resonators, Phys. Rev. Lett. **113**, 110502 (2014).
[30] D. L. Sounas and A. Alù, Time-Reversal Symmetry Bounds on the Electromagnetic Response of Asymmetric Structures, Phys. Rev. Lett. **118**, 154302 (2017).
[31] Y. Shi, Z. Yu, and S. Fan, Limitations of nonlinear optical isolators due to dynamic reciprocity, Nat. Photonics **9**, 388 (2015).